




Compressed Wideband Spectrum Mapping in 3D Spectrum-Heterogeneous Environment

Feng Shen , Guoru Ding , Senior Member, IEEE, Qihui Wu , Senior Member, IEEE, and Zheng Wang, Member, IEEE

Abstract—Given the explosive growth of wireless devices ranging from the 2D ground to the 3D space, the first task preceding any form of dynamic spectrum management for the smart city infrastructures is the sensing of heterogeneous spectrum situation in wireless environments. However, challenge arises when increasing wide bandwidth and enormous geographic space meet power-limited CR receivers with constrained hardware capability. In this paper, a 3D compressed wideband spectrum mapping model is established by exploiting the underlying sparse nature of wideband spectrum situation based on compressed sensing, where joint time-frequency-space compression is executed at sub-Nyquist sampling rate. Due to the ineffectiveness of traditional algorithms, a novel two-phase 3D compressed wideband spectrum mapping scheme is proposed which is composed of sampling points optimization and 3D wideband spectrum situation recovery. Therein, quadrature and right-triangular (QR) block pivoting based spatial sampling matrix optimization algorithm considers every frequency priority of each location jointly to select dominant sampling locations. Alternating direction method of multipliers is further applied to iteratively solve the situation recovery. Lastly, in-depth numerical simulations demonstrate the spectrum situation recovery performance, which proves the proposed 3D compressed wideband spectrum mapping scheme greatly reduces the number of measurements, while achieving a high level of wideband spectrum mapping accuracy.

Index Terms—Wideband spectrum mapping, compressed sensing, QR factorization, spectrum-heterogeneity.

I. INTRODUCTION

A. Background and Motivation

WITH the rapid development of wireless communications, ubiquitous wireless devices have been widely applied in various fields, which cause crowded spectrum environment and bring the scarcity of spectrum resources an urgent problem [1], [2], [3]. However, the Federal Communications Commission (FCC) reports that large amounts of spectrum are underutilized,

including broadcasting TVs and analogue cellular telephony, etc. [4], [5]. Therefore, how to efficiently utilize spectrum resources has received much attention. Cognitive radio (CR) [6], [7], [8], [9], [10], [11] is the first spectrum sharing technology, of which spectrum sensing plays a fundamental role in detecting spectrum holes that can be used by secondary users (SUs) without interfering with primary users (PUs). In the DARPA RadioMap program [12], spectrum situation awareness is introduced. As the name implies, spectrum situation describes the state of the wireless environment, which includes spectrum occupancy state, signal strength, modulation mode, and access protocol, etc. Due to the difference in signal source distribution, channel attenuation and shadowing, different spatial locations and frequency points will exhibit a variety of spectrum access opportunities, which is referred to as spectrum heterogeneity.

Spectrum mapping aims to create a spectrum map based on spectrum situation awareness. It enables us to associate the awareness results with three-dimensional (3D) geographic coordinates accordingly. With the help of the spectrum map, radio frequency (RF) devices can access the idle spectrum and avoid interference where it is busy. Spectrum situation awareness results are continuously shared by RF sensors [13], allowing the spectrum map to be updated over time. In spectrum-heterogeneous environments with limited spectrum resource, this will increase the number of RF devices and the amount of communications, which will undoubtedly improve spectrum utilization [14] in the space-frequency-time domain.

Recently, wideband spectrum sensing has been widely applied, collecting wideband signals with high-speed analog-to-digital converters (ADCs). Quan et al. [15] propose a multi-band joint detection algorithm that uses high-speed ADC for signal acquisition and analyzes the occupancy of the PU. Wavelet-based broad spectrum sensing is studied by Tian and Giannakis [16] with the aid of high-speed ADC. Nyquist sampling theory states that the sampling rate must be at least twice the signal bandwidth. For a receiver with limited power and hardware capability, Nyquist rate sampling is virtually impossible when the spectrum being monitored has very wide bandwidth. To ensure stable reconstruction of multi-band signals, Landau [17] proves that the sampling rate should not be smaller than the measured value of the occupied part of the spectrum, which is often less than the Nyquist sampling rate.

With the sparsity property of the underutilized spectrum, sub-Nyquist rate sampling with compressive sensing is proposed for wideband spectrum processing. Compressed sensing (CS) [18],

Manuscript received 5 October 2022; accepted 1 December 2022. Date of publication 6 December 2022; date of current version 18 April 2023. This work was supported in part by the National Natural Science Foundation of China under Grants 61827801, 61871398, and 61931011 and in part by the Natural Science Foundation for Distinguished Young Scholars of Jiangsu Province of China under Grant BK20190030. The review of this article was coordinated by Prof. Yue Gao. (Corresponding author: Qihui Wu.)

Feng Shen and Qihui Wu are with the College of Electronics and Information Engineering, Nanjing University of Aeronautics and Astronautics, Nanjing 211106, China (e-mail: sfjx_nuaa@163.com; wuqihui2014@sina.com).

Guoru Ding is with the College of Communications Engineering, Army Engineering University, Nanjing 210007, China (e-mail: dr.guoru.ding@ieee.org).

Zheng Wang is with the School of Information Science and Engineering, Southeast University, Nanjing 210096, China (e-mail: z.wang@ieee.org).

Digital Object Identifier 10.1109/TVT.2022.3227168

[19], [20], [21], [22], also known as compressed sampling, has been widely applied in various fields such as electronic engineering, image processing, wireless communication and so on. By contrast with Nyquist theory in signal processing, compressed sensing method employs random sampling to obtain discrete samples of the signal, and then reconstructs the signal through a nonlinear reconstruction algorithm. By exploiting the sparseness of the signal, compressed sensing can achieve high signal reconstruction performance even with only a few measurements. This is consistent with our goal to estimate the entire three dimensional wideband spectrum situation map through a few spectrum sampling points. In addition, the spatial diversity of the transceivers can also be used to allocate the entire frequency band to multiple users, so that the spectrum sampling cost for each transceiver will be reduced, thereby improving the sampling efficiency.

Therefore, these observations motivate us in this paper to consider how to exploit the sparse nature of the 3D wideband spectrum situation, optimize sampling points and recover the spectrum situation in the entire 3D wideband spectrum-heterogeneous space with compressed sensing theory.

B. Related Work

Currently, few studies have been conducted on 3D wideband spectrum mapping. The authors in [23] present a radio environment map (REM) based on data extracted from heterogeneous spectrum sensors, which describes how a radio environment map can be constructed for spectrum management. According to [24], kernel-based learning and nonlinear support vector machine (SVM) are applied to identify the PU coverage boundaries, which can be viewed as a two-dimensional binary spectrum map. Using SVM-type solvers, the work [25] decreases the bandwidth requirement for sensor measurements by introducing linear compression and quantization. Moreover, the authors in [26] present an algorithm for estimating the power spectrum through generative adversarial networks (GANs). A regression model is established with deep learning, and image color mapping is used to transform the estimation task into image reconstruction. In [27] and [28], an idea of image inference is proposed to complete the spectrum situation of multiple frequency points across multiple time slots. However, these studies do not combine the spectrum data with the practical three-dimensional geographical scenario as described in [29]. Recent work [30] explores 3D spectrum mapping based on region of interest (ROI). It is intended to spend less energy and improve ROI spectrum situation recovery at the same time. But it doesn't take into account the internal mechanisms of signal propagation characteristics, which is listed as an open issue. In [31], it discovers that by quadrature and right-triangular (QR) factorization with column pivoting, an optimal sensor placement may be achieved through features extracted from training data. This is agreed with our goal, which is to accurately reconstruct the entire 3D spectrum situation map with the minimum optimal sampling points.

What's more, since compressed sensing was proposed in [19], [32], it has been widely applied in various theoretical studies and

practical applications. It breaks the limitation of the traditional Nyquist sampling theorem, and can reconstruct the original signal with less sampling without distortion, which greatly reduces the measurement cost. The three major problems of compressed sensing are the establishment of sparse dictionary, the optimization of sampling matrix and the sparse signal recovery algorithm. The articles [33], [34] study the restricted isometric property (RIP) and [35] proposes the incoherence of sensing matrix and sparse dictionary. They all characterize the correlation between the sensing matrix and the sparse matrix. It is shown that by reducing the correlation, the compressed sensing reconstruction error and the required observations for accurate reconstruction can be reduced.

Y. Wang et al. [36] propose a spectrum sensing scheme in which each CR monitors only a segment of the entire spectrum and samples at a reduced Nyquist rate in the time domain with compressed sensing. In our recent work [37], a first attempt to explore spectrum mapping based on compressed sensing is carried out. However, only sparse sampling in the space domain is considered, which motivates us to extend our research into joint space-time-frequency compression. Based on Nyquist sampling theory, Tian [21] introduces CS to wideband spectrum sensing, where fewer compressed measurements are required. Sun et al. [38] propose to adjust the compressed measurements adaptively in continuous sensing slots. However, it brings great computational complexity since signal reconstruction has to be repeated several times until the proper signal recovery is reached. Wideband spectrum sensing algorithms are presented by Qin et al. [39], [40] for both single node and multiple nodes, which are evaluated on the TV white space to enable dynamic spectrum access.

In a nutshell, it is observed that, even though spectrum mapping has been studied, most of the existing studies focus on spectrum map of the 2D ground for a specific frequency point, which doesn't match the actual wideband spectrum in the 3D spectrum heterogeneous environment. What's more, the existing works take the construction of spectrum maps as matrix completion with missing values [27], [28]. However, matrix completion only adapts to signals of single domain or joint domains without domain transformation. In wideband spectrum mapping, it involves time-frequency transformation in signal acquisition, failing to apply matrix completion method as well as our recovery algorithm in [37]. Meanwhile, in order to save time and reduce sampling cost, how to execute joint compression of space, frequency and time for wideband spectrum mapping emerges as a new challenge as well. Moreover, the existing works [41], [42] usually perform random sampling, there are few studies on optimizing the sampling points of wideband spectrum mapping. Intuitively, if the sampling points can better exploit the intrinsic features of the entire spectrum situation, we can achieve the same performance as random sampling with fewer sampling points. To address these issues and challenges, we will investigate 3D compressed wideband spectrum mapping with optimized sampling points in spectrum-heterogeneous environments by leveraging the underlying sparse nature of the 3D wideband spectrum situation.

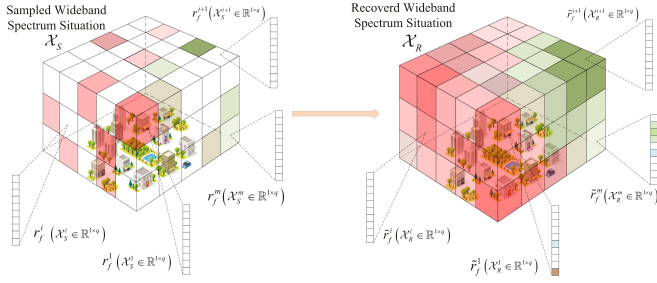


Fig. 1. Graphical illustration of 3D wideband spectrum mapping. The left \mathcal{X}_S and the right \mathcal{X}_R display the sampled and recovered wideband spectrum situation, respectively. $\mathcal{X}_S^i \in \mathbb{R}^{1 \times q}$ and $\mathcal{X}_R^i \in \mathbb{R}^{1 \times q}$ represent the sampled and recovered q -length frequency vectors at the i -th geographical position. The spectrum mapping task is to accurately recover the spectrum situation values for every frequency point at every discretized geographical location through a limited number of sampling points.

C. Contributions

The main contributions of this paper are summarized as follows:

- The 3D compressed wideband spectrum mapping model is first formulated as a compressed sensing optimization problem in the space, frequency and time domains simultaneously, by exploiting the joint sparsity in space and frequency.
- A QR block pivoting based spatial sampling points optimization is proposed as the first phase of the overall 3D compressed wideband spectrum mapping scheme. Therein, the priorities of every frequency point at each location are taken into account to ensure the superiority of selected locations.
- Alternating direction method of multipliers based 3D wideband spectrum situation reconstruction is developed as the second phase, which brings excellent spectrum situation recovery performance against the ineffective traditional algorithms.

The rest of this paper is organized as follows. In Section II, 3D wideband spectrum mapping is introduced and the 3D compressed wideband spectrum mapping model is formulated. The two-phase 3D compressed wideband spectrum mapping scheme is subsequently proposed in Section III. Simulation results are presented in Section IV, and conclusions are drawn in Section V.

II. SYSTEM MODEL AND PROBLEM FORMULATION

This paper addresses the construction of a 3D wideband spectrum map as shown in Fig. 1. The spectrum power strengths of different frequency points at different positions varies since signal sources exist randomly in the 3D space. The position with frequent communication behaviors indicates high spectrum power strength (in red), and the idle position far away from the signal sources indicates low spectrum power strength (in green). Therefore, the entire 3D area to be monitored is spectrum-heterogeneous. Obtaining a complete and accurate 3D wideband spectrum situation map is the goal of 3D wideband spectrum mapping, through which we can get the spectrum occupancy and channel quality of any frequency at any position so that dynamic

spectrum access management can be carried out efficiently and reliably. Fig. 1 shows the 3D space can be discretized into a spectrum tensor $\mathcal{X} \in \mathbb{R}^{N_1 \times N_2 \times N_3 \times q}$ in both space and frequency domains, where N_1 , N_2 , and N_3 denote the grid number of the target 3D space in x , y , z dimensions, q is the frequency points number.

A. Preliminaries on 3D Wideband Spectrum Mapping

Normally, spectrum mapping is supposed to execute power strength measurements at every point and it will undoubtedly obtain an accurate spectrum map. However, it will suffer enormous resource consumption. Therefore, the complete 3D wideband spectrum map should be obtained by measuring the signal at as few points as possible and recovering all unsampled points as shown in Fig. 1. To avoid blind sampling, it is necessary to find suitable spatial sampling positions as well as frequency points. Moreover, by taking advantage of the correlations among the sampling points, it is able to restore the spectrum situation with limited sampling data. Of course, a very small sampling ratio will also severely destroy the relationships among all the sampling points, resulting in poor spectrum situation recovery. Additionally, even with the same sampling ratio, different combinations of sampling points will yield different recovery accuracies [30].

The objective is, therefore, to optimize space and frequency sampling points in order to achieve better reconstruction of wideband spectrum situations with limited sampling ratio as follows:

$$\Theta^* = \arg \min_{\Theta \subseteq \mathcal{X}} W_{\mathcal{X}}, \quad (1)$$

$$\text{s.t. } r = \frac{N_{\Theta}}{N_1 \cdot N_2 \cdot N_3 \cdot q}, \quad (\text{C1} - 1)$$

$$W_{\mathcal{X}} = \frac{1}{N_{\mathcal{X}}} \sum_{i,j} \left(\frac{|\mathcal{X}_R^{ij} - \mathcal{X}^{ij}|}{\mathcal{X}^{ij}} \right)^2, \quad (\text{C1} - 2)$$

where Θ denotes a set of sampling points, including the selected sampling positions and the chosen frequency points of every position. $W_{\mathcal{X}}$ represents the relative mean square error (RMSE) of the recovered 3D wideband spectrum situation \mathcal{X} . N_{Θ} is the sampling number, and r is the sampling ratio. $N_{\mathcal{X}} = N_1 \times N_2 \times N_3 \times q$ corresponds to the total points number of \mathcal{X} . \mathcal{X}^{ij} and \mathcal{X}_R^{ij} denote the original and estimated spectrum power strength of the j -th frequency point at the i -th position, respectively. Traditionally, researchers usually treat spectrum mapping problem as a matrix completion problem by decomposing the tensor into matrices to recover [27], [28]. However, matrix completion is not applicable to wideband spectrum mapping due to the time and frequency domain transformation in signal acquisition and processing. What's more, a large $N_{\mathcal{X}}$ will output a total of $\frac{N_{\mathcal{X}}!}{(r \cdot N_{\mathcal{X}})!((1-r) \cdot N_{\mathcal{X}})!}$ solutions for a given sampling ratio r , which is nearly impossible to achieve by exhaustive searching. Therefore, it is of paramount importance to conduct in-depth research on reduction of sampling number and optimization of sampling points.



Fig. 2. 3D compressed wideband spectrum mapping model. SS_j represents the j -th signal source (there may be a real signal source or no signal source) of all n positions, the UAV equipped with a spectrum monitoring device flies to m out of n positions to sense p out of q frequency points at each position.

B. 3D Compressed Wideband Spectrum Mapping Model and Formulation

Consider a wide frequency band scene in a city block that covers many signal sources as shown in Fig. 2. Let i and j denote two different geographic location indexes ($i \neq j$) in the 3D space. The i -th location refers to the i -th sampling position (SP_i), and the j -th location refers to the j -th signal source position (SS_j). For the convenience of signal processing, it is supposed that the overall wideband of system is slotted into q non-overlapping bins of equal bandwidth. These frequency bins are termed as channels and indexed by $[1, 2, \dots, q-1, q]$. Moreover, the entire $N_1 \times N_2 \times N_3$ situation tensor \mathcal{X} of the 3D geographical space is vectorized into $\mathbf{r} \in \mathbb{R}^{n \times 1}$ ($N_1 = N_2 = N_3 = N, n = N^3$). In order to quickly sample the target positions, unmanned aerial vehicle (UAV) with an onboard spectrum monitoring device can hover at the exact position to sense the spectrum power strength of multiple frequency points, and then fly to the next position, alleviating the inconvenience of device movement in three-dimensional space.

Let $\mathbf{s}_f^j \in \mathbb{R}^{1 \times q}$ denote the unknown transmitted power strength of the signal sources at the j th position. Therefore, by stacking $\mathbf{s}_f^j, j = 1, 2, \dots, n$ in the 3D space, a sparse signal source matrix $\mathbf{S} \in \mathbb{R}^{n \times q}$ can be obtained. Assuming the signal sources are sparsely located at only \tilde{k} out of n positions, thereby the sparsity is $k = \|\mathbf{S}\|_0 = \tilde{k}q$, which measures the number of the nonzero elements of \mathbf{S} , in other words, of tensor \mathcal{X} . Therefore, for any possible SP_i , the received signal power strength is

$$\mathbf{r}_f^i = \sum_{j=1}^n h_{ij} \mathbf{s}_f^j T, \quad (2)$$

which represents the linear superposition of signals from all positions in the 3D space. h_{ij} is the signal attenuation coefficient which will be later defined in (8). $\mathbf{s}_f^j T$ is the transpose of \mathbf{s}_f^j ,

where $\mathbf{s}_f^j = [s_{f_1}^j, s_{f_2}^j, \dots, s_{f_q}^j] \in \mathbb{R}^{1 \times q}$ satisfies

$$s_{f_v}^j = \begin{cases} p_{f_v}, & \text{if } f_v \text{ of position } j \text{ is occupied,} \\ 0, & \text{else.} \end{cases} \quad (3)$$

It should be noted that we do not know the position of the signal source in a real physical environment, so at the j -th location, it may have a real signal source (transmission power is p_{f_v}) or no signal source (transmission power is 0). p_{f_v} is the signal transmit power of frequency f_v . $s_{f_v}^j$ is the v -th element of \mathbf{s}_f^j .

To characterize the building blocking and fading in real spectrum environment, both LOS and NLOS propagation scenarios should be taken into account which have been studied in [43]. Considering a three-dimensional space, we have to consider air-to-air path along with air-to-ground path, resulting in the channel model as follows:

The path loss for line-of-sight (LoS) and non-line-of-sight (NLoS) links between location i (frequency v) and j (frequency v') is given as

$$\Gamma_{ij}^{vv'} = \begin{cases} \eta_1 (4\pi f_c d_{ij}^{vv'} / c)^\varpi, & \text{LoS,} \\ \eta_2 (4\pi f_c d_{ij}^{vv'} / c)^\varpi, & \text{NLoS,} \end{cases} \quad (4)$$

where f_c is the carrier frequency. c is the light speed. ϖ is the path loss exponent of spectrum environment. η_1 and η_2 represent the excessive path loss coefficients in LoS and NLoS links, respectively. $d_{ij}^{vv'}$ denotes the Euclidean distance between location i (frequency v) and j (frequency v'), it is defined as:

$$d_{ij}^{vv'} = \|\mathcal{X}_{f_v}^i - \mathcal{X}_{f_{v'}}^j\|_2, i \neq j \quad (5)$$

$\mathcal{X}_{f_v}^i$ and $\mathcal{X}_{f_{v'}}^j$ are the i -th and j -th geographical locations with frequency v and v' respectively in the Cartesian coordinate. The overall path loss is obtained by averaging the link probabilities as

$$\bar{\Gamma}_{ij}^{vv'} = P_{ij}^{vv',LOS} \Gamma_{ij}^{vv',LOS} + P_{ij}^{vv',NLOS} \Gamma_{ij}^{vv',NLOS}, i \neq j, \quad (6)$$

where $P_{ij}^{vv',LOS}$ and $P_{ij}^{vv',NLOS}$ represent the LOS and NLOS probabilities, respectively. $P_{ij}^{vv',LOS} = 1 - P_{ij}^{vv',NLOS}$ and

$$P_{ij}^{vv',LOS} = \min \left\{ \frac{e^{\tau \cdot \min\{z_{f_v}^i, z_{f_{v'}}^j\}}}{1 + \alpha \exp(-\beta [\frac{180}{\pi} \theta_{ij}^{vv'} - \alpha])}, 1 \right\}, i \neq j. \quad (7)$$

$z_{f_v}^i$ and $z_{f_{v'}}^j$ are the heights of location i (frequency v) and j (frequency v'), $e^{\tau \cdot \min\{z_{f_v}^i, z_{f_{v'}}^j\}}$ is a coefficient which helps to refine the air-to-ground channel in [43] to cover the air-to-air channel as well. This reasonable assumption is based on the fact that the closer one of the location i or j is to the ground, the smaller the probability of LOS signal propagation will be. In other words, the smaller $z_{f_v}^i$ or $z_{f_{v'}}^j$ is, the closer $e^{\tau \cdot \min\{z_{f_v}^i, z_{f_{v'}}^j\}}$ is to 1, which becomes the original air-to-ground channel model. τ is used to adjust the influence of $z_{f_v}^i$ and $z_{f_{v'}}^j$. The larger the τ is, the greater the possibility of LOS propagation is. Parameters α and β are determined by the environment. $\theta_{ij}^{vv'}$ denotes the elevation angle between location i (frequency v) and j (frequency v').

Specifically, when $i = j$, it means that the i -th sampling position is exactly at the j -th signal source, so the measured spectrum power strength is considered to be the transmission power of the signal source (or if there is no signal source, the transmission power is 0). In other words, there is no signal transmission attenuation, so we set $h_{ij} = 1$ if $i = j$. Consequently, the spectrum power strength fading coefficient at any point in 3D space comes as:

$$h_{ij} = \begin{cases} \left(\tilde{\Gamma}_{ij}^{vv'}\right)^{-1}, & i \neq j, \\ 1, & i = j. \end{cases} \quad (8)$$

It's noting that $h_{ij}^{vv'}$ are the same for $\forall v, v'$, so h_{ij} is adopted for simplicity.

Let us stack all measurement vectors $\{\mathbf{r}_f^i\}$ into a single vector

$$\mathbf{r}_f = [\mathbf{r}_f^1; \mathbf{r}_f^2; \dots; \mathbf{r}_f^{n-1}; \mathbf{r}_f^n], \quad (9)$$

and stack all $\{s_f^i\}$ into

$$\mathbf{s}_f = [s_f^{1T}; s_f^{2T}; \dots; s_f^{n-1T}; s_f^{nT}], \quad (10)$$

we can obtain

$$\mathbf{r}_f = \mathbf{H}\mathbf{s}_f, \quad (11)$$

where

$$\mathbf{H}_{ij} = \text{diag}(\text{repmat}(h_{ij}, [1, q])), \quad (12)$$

$$\mathbf{H} = \begin{pmatrix} \mathbf{H}_{11} & \dots & \mathbf{H}_{1n} \\ \vdots & \ddots & \vdots \\ \mathbf{H}_{n1} & \dots & \mathbf{H}_{nn} \end{pmatrix}. \quad (13)$$

$\mathbf{H} \in \mathbb{R}^{nq \times nq}$ is constructed by n^2 diagonal matrix \mathbf{H}_{ij} . $\text{repmat}(\cdot)$ returns a larger matrix containing several copies of the original matrix in the row and column dimensions. $\text{diag}(\cdot)$ creates a diagonal matrix with the given elements.

Suppose m locations are sampled, it brings a spatial compression $r_S = m/n$. Thus, we obtain the space compressed signal as:

$$\mathbf{r}_f^{SC} = \mathbf{L}\mathbf{r}_f, \quad (14)$$

where

$$\mathbf{L} = \begin{pmatrix} \mathbf{L}_{11} & \dots & \mathbf{L}_{1n} \\ \vdots & \ddots & \vdots \\ \mathbf{L}_{m1} & \dots & \mathbf{L}_{mn} \end{pmatrix}, \quad (15)$$

$$\mathbf{L}_{ij} = \begin{cases} \mathbf{I}, & \mathcal{X}_f^j \text{ is the } i\text{th sampled location,} \\ \mathbf{0}, & \text{location } \mathcal{X}_f^j \text{ is not sampled,} \end{cases} \quad (16)$$

$\mathbf{L}_{ij} \in \mathbb{R}^{q \times q}$ is either unit matrix $\mathbf{I}_{q \times q}$ or zero matrix $\mathbf{0}_{q \times q}$, which represent the two states "sampled" and "unsampled" of the j th position, respectively. Each row of \mathbf{L} at most has an element of \mathbf{I} , which reveals the chosen position.

As discussed in the Section I, the cognitive radio users may have frequency-agile transceivers. However, due to the transceiver volume and power consumption limitations, we let the transceiver only collect p out of q frequency points rather

than the entire spectrum. Thus, the frequency sampling ratio is compressed by $r_F = p/q$, and the joint frequency and space compressed signal is:

$$\mathbf{r}_f^{FSC} = \mathbf{D}\mathbf{r}_f^{SC}, \quad (17)$$

where

$$\mathbf{D} = \begin{pmatrix} \mathbf{D}_{11} & \dots & \mathbf{D}_{1n} \\ \vdots & \ddots & \vdots \\ \mathbf{D}_{m1} & \dots & \mathbf{D}_{mn} \end{pmatrix}. \quad (18)$$

Specifically, $\mathbf{D}_{ij} \in \mathbb{R}^{p \times q}$ results from a $q \times q$ identity matrix $\mathbf{I}_{q \times q}$ by keeping only q rows whose indices represent the chosen frequency points, which satisfies $\mathbf{D}_{ij} = \mathbf{0}$ if $\mathbf{L}_{ij} = \mathbf{0}$, as well as

$$\mathbf{D}_{ij}^v = \begin{cases} 1, & \text{frequency } f_v \text{ of location } \mathcal{X}_f^j \text{ is sampled,} \\ 0, & \text{frequency } f_v \text{ is not sampled.} \end{cases} \quad (19)$$

Furthermore, when Nyquist rate sampling is adopted at SP_i , it collects discrete-time sample vector in the form of

$$r_t^{TFSC,i} = \mathbf{G}_i^{-1} r_f^{FSC,i}, \quad (20)$$

where $\mathbf{G}_i \in \mathbb{R}^{p \times p}$ is the square discrete Fourier transform (DFT) matrix. \mathbf{G}_i^{-1} is the inverse matrix of \mathbf{G}_i . $r_f^{FSC,i}$ is the i th q -length segment of the frequency and space compressed signal $r_f^{FSC} \in \mathbb{R}^{mp \times 1}$. $r_t^{TFSC,i}$ is also the i th q -length segment of the whole discrete-time sample vector r_t^{TFSC} .

Let

$$\mathbf{G}_{1:m}^{-1} = [\mathbf{G}_1^{-1}, \mathbf{G}_2^{-1}, \dots, \mathbf{G}_{m-1}^{-1}, \mathbf{G}_m^{-1}], \quad (21)$$

the complete discrete-time sample vector becomes:

$$r_t^{TFSC} = \text{diag}(\mathbf{G}_{1:m}^{-1}) r_f^{FSC}. \quad (22)$$

At last, time compressed sampling is executed at the selected SP_i which amounts to imposing an Gaussian random matrix $\Phi_i \in \mathbb{R}^{u \times p}$ to collect compressive linear projections from the q -length vector $r_t^{TFSC,i}$, with the time compression ratio $r_T = u/p$. The non-compression case of time domain corresponds to $u = p$. Similarly to $\mathbf{G}_{1:m}^{-1}$, we have

$$\Phi_{1:m} = [\Phi_1, \Phi_2, \dots, \Phi_{m-1}, \Phi_m], \quad (23)$$

and the final received signal is

$$\mathbf{y} = \text{diag}(\Phi_{1:m}) r_t^{TFSC}. \quad (24)$$

Putting together, we summarize the whole signal processing as follows:

$$\mathbf{y} = \Phi \mathbf{G} \mathbf{D} \mathbf{L} \mathbf{H} \mathbf{s}_f + \boldsymbol{\varepsilon}, \quad (25)$$

where $\mathbf{G} = \text{diag}(\mathbf{G}_{1:m}^{-1}) \in \mathbb{C}^{mp \times mp}$, $\Phi = \text{diag}(\Phi_{1:m}) \in \mathbb{C}^{mu \times mp}$, $\mathbf{y} \in \mathbb{C}^{mu \times 1}$, $\boldsymbol{\varepsilon}$ is the complex Gaussian additive white noise with power spectral density σ_0^2 .

At present, the application of compressed sensing to wideband 3D spectrum mapping has not been researched. The difficulty lies in exploiting the inherent sparsity feature of 3D wideband spectrum situation. In fact, compared with the total discretized points in the entire large situation tensor \mathcal{X} , occupied frequencies

in both space and frequency domains are sparse. Hence, 3D wideband spectrum mapping has the following objective:

$$\min \|\mathbf{y} - \Phi \mathbf{G} \mathbf{D} \mathbf{L} \mathbf{H} \mathbf{s}_f\|_2^2 + \lambda \|\mathbf{s}_f\|_1. \quad (26)$$

III. TWO-PHASE 3D COMPRESSED WIDEBAND SPECTRUM MAPPING SCHEME

This section introduces a two-phase compressed spectrum mapping scheme for solving the 3D space-frequency-time compressions and situation recovery problem, based on compressed sensing theory and alternating direction method of multipliers (ADMM) method. The two phases include spatial sampling matrix optimization and 3D wideband spectrum situation reconstruction.

A. QR Block Pivoting Based Spatial Sampling Matrix Optimization

Generally, the coherence between different frequency points is weak, so that random frequency point selection is adopted for each spatial position. However, according to the law of signal propagation, the 3D wideband spectrum situation is highly correlated in the spatial domain, so the selection of the spatial sampling position has a greater impact on the accuracy of situation recovery. Intuitively, if the selected sampling locations can better exploit the intrinsic features of the entire 3D spatial spectrum situation, the same performance as random sampling can be achieved even with fewer sampling locations. Therefore, we will optimize the spatial sampling matrix first.

The QR decomposition is one of the most well known and useful tools in numerical linear algebra. A matrix \mathbf{G} can be decomposed into an orthogonal matrix \mathbf{Q} and a right triangle matrix \mathbf{R} , that is $\mathbf{G} = \mathbf{Q}\mathbf{R}$, however, this standard QR algorithm is not appropriate for purposes such as rank determination or low rank estimations. According to [44], [45], column permutation is helpful to find more representative columns, where a permutation matrix \mathbf{P} is introduced to rearrange columns into a more beneficial ordering as $\mathbf{G}\mathbf{P} = \mathbf{Q}\mathbf{R}$. It is named as QR decomposition with column pivoting, which has various applications such as least-squares approximation discussed in [46], [47], as well as measurement selection tasks [31], [48].

In (25), the invertibility of $\Phi \mathbf{G} \mathbf{D} \mathbf{L} \mathbf{H}$ has a greater impact on the recovery of the sparse signal \mathbf{s}_f , which can be measured by the condition number of a matrix. The condition number refers to the ratio of maximum and minimum singular values, and is indirectly bounded by optimizing a matrix's spectral content such as its determinant, trace, or spectral radius. In [31], the oversampled sensor placement problem is studied, where the sensor number is larger than the mode number for reconstruction ($\tilde{m} > \tilde{r}$, \tilde{r} is the rank of the tailored \mathbf{H}). The key idea to enable oversampling is the QR factorization in combination with column pivoting to generate \tilde{r} sensors (pivots) that effectively sample the \tilde{r} basis modes of \mathbf{H} :

$$\mathbf{H}^T \mathbf{C}^T = \mathbf{Q}\mathbf{R}. \quad (27)$$

Here the column permutation matrix \mathbf{C} represents the sensor placement matrix and is optimized by maximizing the matrix

Algorithm 1: QR Block Pivoting Based 3D Wideband Spectrum Mapping Spatial Sampling Matrix Optimization.

Input:

3D wideband spectrum mapping sparse representation matrix \mathbf{H} ; Sampling number m ; Initial selected column index set $\gamma = \emptyset$;

Output:

Column priority set γ ; The optimized 3D wideband spectrum mapping spatial sampling matrix \mathbf{L} ;

- 1: Initialize $\mathbf{A}_0 = \mathbf{H}$;
 - 2: **for** $j = 1; j \leq nq; j++$ **do**
 - 3: Compute column 2-norms of \mathbf{A}_{j-1} and find the column index $\gamma_j = \arg \max_{j \notin \{1, 2, \dots, j-1\}} \|\mathbf{a}_j\|_2$, where $\mathbf{a}_j = (a_{jj}, a_{(j+1)j}, \dots, a_{(nq)j})^T$;
 - 4: Apply permutation matrix \mathbf{S}_j to swap j -th column with γ_j -th column;
 - 5: Establish Householder reflection on the current j -th column: $\tilde{\mathbf{H}}_j \cdot \mathbf{a}_j = (|\mathbf{a}_j|, 0, \dots, 0)^T$, where $\tilde{\mathbf{H}}_j = \mathbf{I} - 2\omega_j \omega_j^T$;
 - 6: Apply reflection and update the trailing columns $\mathbf{A}_j = \text{diag}(\mathbf{I}_{j-1}, \tilde{\mathbf{H}}_j) \cdot \mathbf{A}_{j-1} \cdot \mathbf{S}_j$ for removing the contribution of row j ;
 - 7: $\gamma = \gamma \cup \{\gamma_j\}$;
 - 8: **end for**
 - 9: $\Upsilon(\gamma[i]) = i, i = 1, 2, \dots, nq$;
 - 10: $\Upsilon_{block,j} = \text{sum}(\Upsilon_{q(j-1)+1:jq}), j = 1, 2, \dots, n$;
 - 11: Select m smallest $\Upsilon_{block,j}$ blocks from the n blocks and denote as Υ_{block}^{opt} ;
 - 12: Output the optimized 3D wideband spectrum mapping measurement matrix \mathbf{L} according to the chosen column index set Υ_{block}^{opt} ;
-

determinant [31]:

$$\gamma^* = \arg \max_{\gamma, |\gamma| = \tilde{m}} |\det \mathbf{M}_\gamma| = \arg \max_{\gamma, |\gamma| = \tilde{m}} \prod_i |\lambda_i(\mathbf{M}_\gamma)|, \quad (28)$$

where $\mathbf{M}_\gamma = \mathbf{C}_\gamma \mathbf{H}_r$ and γ stores the indexes of m selected columns. $\det(\cdot)$ calculates the matrix determinant and λ_i represents the eigenvalue of \mathbf{M}_γ .

According to (27) and (28), we obtain

$$\begin{aligned} \max |\det(\Phi \mathbf{G} \mathbf{D} \mathbf{L} \mathbf{H})| &= \max |\det(\Phi \mathbf{G} \mathbf{D})| |\det(\mathbf{L} \mathbf{H})| \\ &= \max |\det(\mathbf{L} \mathbf{H})| = \max |\det(\mathbf{Q}\mathbf{R})| \\ &= \max |\det \mathbf{Q}| |\det \mathbf{R}| = \max |\det \mathbf{R}| \\ &= \max \prod_i |a_{ii}|. \end{aligned} \quad (29)$$

Therefore, we have:

$$\mathbf{H}^T \mathbf{L}^T = \mathbf{Q}\mathbf{R}. \quad (30)$$

In other words, the goal of maximizing the first \tilde{m} eigenvalues of matrix \mathbf{M}_γ can be achieved by maximizing the first \tilde{m} diagonal items of matrix \mathbf{R} .

The QR pivoting algorithm is an approximate greedy solution, also known as submatrix volume maximization (here, matrix

volume is the absolute value of the determinant). Iteratively, the submatrix volume is increased by selecting a new dominant column with the maximum 2-norm:

$$\gamma_j = \arg \max_{j \notin \{1, 2, \dots, j-1\}} \|\mathbf{a}_j\|_2. \quad (31)$$

Then, the dominant column is altered by applying the Householder transformation

$$\tilde{\mathbf{H}}_j \cdot \mathbf{a}_j = (|\mathbf{a}_j|, 0, \dots, 0)^T, \quad (32)$$

where $\tilde{\mathbf{H}}_j = \mathbf{I} - 2\omega_j\omega_j^T$ is called reflection vector as follows:

$$\omega_j = \frac{\hat{\mathbf{a}}_j - |\hat{\mathbf{a}}_j| \mathbf{e}}{|\hat{\mathbf{a}}_j - |\hat{\mathbf{a}}_j| \mathbf{e}|}. \quad (33)$$

Therein $\hat{\mathbf{a}}_j$ refers to the column with the maximum 2-norm in the j -th iteration. The unit vector \mathbf{e} is the same length as $\hat{\mathbf{a}}_j$, with 1 at the first index and zeros elsewhere. To further subtract the Householder contributions from every other column onto the pivot column, $\text{diag}(\mathbf{I}_{j-1}, \tilde{\mathbf{H}}_j)$ is multiplied.

By enforcing a diagonal dominance structure, the above procedure recomputes and gradually expands the submatrix volume for each new column selection [49]. As a result, after nq iterations, the priority vector $\Upsilon \in \mathbb{R}^{nq \times 1}$ for all frequency points in space (the smaller the Υ_j , the higher the priority) is calculated. Since the priorities of different frequency points at different locations are different, we calculate the block priority for each of the n locations given the spatial sampling rate $r_S = m/n$. Specifically, the block priority of the j -th location is the sum of the priorities of the q frequency points at this location, namely $\Upsilon_{\text{block},j}$,

$$\Upsilon_{\text{block},j} = \text{sum}(\Upsilon_{q(j-1)+1:jq}), j = 1, 2, \dots, n. \quad (34)$$

Finally m optimal positions are selected from n spatial positions according to $\Upsilon_{\text{block},j}$ and denoted as $\Upsilon_{\text{block}}^{\text{opt}}$. Therefore the spatial sampling matrix \mathbf{L} is generated in this way: When the j -th (out of n) position is sampled as the i -th (out of m) chosen location, the $((j-1)q+1)$ -th to jq -th rows of an $nq \times nq$ unit matrix are taken as the $((i-1)q+1)$ -th to iq -th rows of the \mathbf{L} matrix ($\mathbf{L} \in \mathbb{R}^{mq \times nq}$).

Algorithm 1 summarizes the entire pseudo implementation code. Lines from 1 to 8 describe the QR pivoting procedures. During each iteration, a pivot is selected with the largest column 2-norm, and the trailing columns are updated to remove the contribution of row j by the Householder transformation. Based on this, we can quickly get the single column priority set γ and then obtain the block priority set $\Upsilon_{\text{block},j}$, which helps to optimize spatial sampling matrix \mathbf{L} for the next spectrum mapping recovery phase.

The time complexity of Algorithm 1 is mainly determined by line 3 and line 6. During the j -th iteration, line 3 has a complexity of $\mathcal{O}((nq-j+1)^2)$. According to matrix multiplication law, the computation cost of line 6 is $\mathcal{O}(2(nq)^3)$. In general, the total time complexity of the QR block pivoting based 3D wideband spectrum mapping measurement matrix optimization is $\mathcal{O}(\sum_{j=1}^{nq} (nq-j-1)^2) + \mathcal{O}(nq(2(nq)^3)) = \mathcal{O}(\frac{nq(nq+1)(2nq+1)}{6} + 2n^4q^4) = \mathcal{O}(n^4q^4)$.

Algorithm 2: ADMM Based 3D Wideband Spectrum Situation Recovery.

Input:

The optimized spatial sampling matrix \mathbf{L} ; Sparse dictionary \mathbf{H} ; The number of iterations K ; Received signal \mathbf{y} ; Frequency sampling matrix \mathbf{D} ; Time sampling matrix Φ ; Frequency-time transformation matrix \mathbf{G} .

Output:

Estimated 3D wideband spectrum situation $\widehat{\mathbf{r}}_f$;

Estimated sparse signal $\widehat{\mathbf{s}}_f$;

- 1: Initialize $\mathbf{z}^{(0)} = \mathbf{0}$, $\boldsymbol{\mu}^{(0)} = \mathbf{0}$, $\mathbf{s}_f^{(0)} = (\Phi\mathbf{GDLH})^\dagger \mathbf{y}$;
 - 2: **for** $j = 1; j \leq K; j++$ **do**
 - 3: Update $\mathbf{s}_f^{(j)}$ as (36);
 - 4: Update $\mathbf{z}^{(j)}$ as (37);
 - 5: Update $\mathbf{w}^{(j)}$ as (38);
 - 6: **end for**
 - 7: Obtain estimated sparse signal $\widehat{\mathbf{s}}_f = \text{abs}(\mathbf{s}_f^{(K)})$;
 - 8: Calculate estimated 3D wideband spectrum situation $\widehat{\mathbf{r}}_f$ as (11);
-

B. ADMM Based 3D Wideband Spectrum Situation Recovery

In this section, based on the optimized spatial sampling matrix \mathbf{L} , we propose a sparsity constrained 3D wideband spectrum situation recovery algorithm based on alternating direction method of multipliers (ADMM) method [50].

We rewrite (26) into augmented Lagrangian form

$$\min \|\mathbf{y} - \Phi\mathbf{GDLH}\mathbf{s}_f\|_2^2 + \lambda \|\mathbf{z}\|_1 + \boldsymbol{\mu}^T (\mathbf{s}_f - \mathbf{z}) + \frac{\rho}{2} \|\mathbf{s}_f - \mathbf{z}\|_2^2, \quad (35)$$

where ρ is the weight parameter controlling the tradeoff between the solution error and the noise tolerance. $\boldsymbol{\mu}$ and \mathbf{z} are the newly introduced variables.

The ADMM turns the multi-variable optimization problem into univariate optimization problem through alternating iterations. Here gradient descent technique is considered and the j -th iterative process is as follows:

$$\mathbf{s}_f^{(j)} = \left((\Phi\mathbf{GDLH})^T \Phi\mathbf{GDLH} + \rho \mathbf{I} \right)^{-1} \times \left((\Phi\mathbf{GDLH})^T \mathbf{y} + \rho (\mathbf{z}^{(j-1)} - \mathbf{w}^{(j-1)}) \right), \quad (36)$$

$$\mathbf{z}^{(j)} = S_{\frac{\lambda}{\rho}} \left(\mathbf{w}^{(j-1)} + \mathbf{s}_f^{(j)} \right), \quad (37)$$

$$\mathbf{w}^{(j)} = \mathbf{w}^{(j-1)} + \mathbf{s}_f^{(j)} - \mathbf{z}^{(j)}, \quad (38)$$

where $\mathbf{w} = \boldsymbol{\mu}/\rho$. $S_{\frac{\lambda}{\rho}}(\cdot)$ represents soft thresholding function, $S_{\frac{\lambda}{\rho}}(\xi) = \frac{\xi}{\text{abs}(\xi)} \max(\text{abs}(\xi) - \lambda, 0)$ and $\xi(\text{abs}(\xi) = 0) = 0$. $\text{abs}(\cdot)$ returns the absolute value of each element for a vector. After desired iterations, we get the estimated sparse signal $\widehat{\mathbf{s}}_f = \text{abs}(\mathbf{s}_f^{(K)})$ where $\mathbf{s}_f^{(j)}$ is complex. Upon (11), the estimated 3D wideband spectrum situation can be finally obtained. The pseudo implementation code is summarized in Algorithm 2.

The time complexity of the proposed ADMM based 3D wideband spectrum situation reconstruction algorithm lies in

updating \mathbf{s}_f in (36). Since $\Phi\mathbf{GDLH} \in \mathbb{C}^{mu \times nq}$, the complexity of $(\Phi\mathbf{GDLH})^T \Phi\mathbf{GDLH} + \rho\mathbf{I}$ is $\mathcal{O}(mu(nq)^2)$. The matrix inversion has complexity of $\mathcal{O}((nq)^3)$. Similarly, the complexity of $(\Phi\mathbf{GDLH})^T \mathbf{y} + \rho(\mathbf{z}^{(j-1)} - \boldsymbol{\omega}^{(j-1)})$ is $\mathcal{O}(nq(mu)^2)$, the complexity of the final multiplication is $\mathcal{O}((nq)^3)$. To sum up, the total computational cost is $\mathcal{O}((nq)^3)$ ($m \ll n, u < q$).

IV. EXPERIMENTAL RESULTS AND DISCUSSIONS

A. Experiment Setup

In this section, numerical simulations are carried out to evaluate the performance of the proposed 3D wideband spectrum mapping scheme. For the scenario setting, a three dimensional city block of $100 \text{ m} \times 100 \text{ m} \times 100 \text{ m}$ is taken into consideration. With a spatial granularity of 12.5 m, the space is discretized into a spectrum tensor of $N_1 \times N_2 \times N_3 = 8 \times 8 \times 8$. The light speed $c = 3 \times 10^8 \text{ m/s}$. The excessive path loss coefficients $\eta_1 = 3 \text{ dB}$ and $\eta_2 = 23 \text{ dB}$. The spectrum loss coefficient $\varpi = 2$. The non-negative parameter $\tau = 0.01$. The environment parameters $\alpha = 11.95$ and $\beta = 0.14$. The frequency points q at each position is 16, which is ranging from 100 MHz–400 MHz, and the interval is 20 MHz, The sparsity \tilde{k} for each frequency point is set to 3. The signal source transmission power is assumed to be 30 mW. The receiver bandwidth is 200 kHz and noise spectral density is -174 dBm/Hz . In order to take into account the unreachable positions due to the buildings, we set up three no-fly cuboid areas, centering at (25 m, 25 m, 12.5 m), (68.75 m, 31.25 m, 12.5 m) and (25 m, 75 m, 12.5 m) with sizes of $25 \text{ m} \times 25 \text{ m} \times 25 \text{ m}$, $37.5 \text{ m} \times 37.5 \text{ m} \times 25 \text{ m}$ and $25 \text{ m} \times 25 \text{ m} \times 25 \text{ m}$.

As comparison algorithms, the compressed sensing based orthogonal matching pursuit (CSOMP) [51] algorithm and generalized orthogonal matching pursuit (GOMP) [52] algorithm are introduced which are two popular sparse signal recovery techniques. When they are applied, the sampling positions in the time-frequency-space domains are derived from random measurements. In addition, the 3D compressed wideband spectrum mapping scheme proposed in Section III is abbreviated as Proposed_TR_FR_SO, which means random Gaussian temporal sampling (TR), random frequency sampling (FR) and optimized spatial sampling (SO). FR refers randomly generating p sampling frequency points from q alternatives in each position. SO represents the desired m sampling positions are optimized according to the block priority in Algorithm 1.

Upon this, two other comparison algorithms are developed, namely Proposed_TR_FS_SO (random Gaussian temporal sampling (TR), sorted frequency sampling (FS) and optimized spatial sampling (SO)) and Proposed_TR_FR_SR (random Gaussian temporal sampling (TR), random frequency sampling (FR) and random spatial sampling (SR)). Sorted frequency sampling (FS) describes a frequency points selection method compared to random selection with the optimized spatial sampling locations. That is, the priority values Υ of the q frequency points at each position j are calculated, and the p frequency points with the highest Υ values are selected as the target sampling frequency points (frequency sampling compression ratio is $r_F = p/q$).

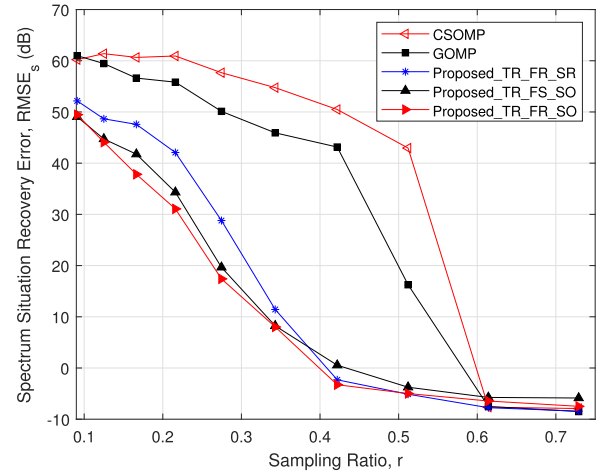


Fig. 3. 3D wideband spectrum situation recovery performance comparisons of the proposed and the comparison algorithms ($r_T = r_F = r_S$).

Besides, SR means the m target sampling locations out of all n candidates are selected at random.

B. Comparison of Situation Recovery Performance

To measure the 3D wideband spectrum situation recovery performance, the average relative situation recovery error $RMSE_s$ of every single frequency at each three-dimensional spatial point is calculated as below:

$$RMSE_s = \frac{1}{nq} \sum_{i=1}^{nq} \left| \frac{\widehat{\mathbf{r}}_f^{(i)} - \mathbf{r}_f^{(i)}}{\mathbf{r}_f^{(i)}} \right|^2, \quad (39)$$

where $\widehat{\mathbf{r}}_f^{(i)}$ and $\mathbf{r}_f^{(i)}$ denote the estimated and true situation values, respectively. The sampling ratio $r = r_T \cdot r_F \cdot r_S$. In Fig. 3, $r_T = r_F = r_S$ is considered. Generally, the spectrum situation recovery error gradually decreases as the sampling rate increases for all algorithms, but our proposed schemes are much more outstanding than the CSOMP and GOMP algorithms. Besides, it is worth noting that the starting performances of CSOMP and GOMP, Proposed_TR_FS_SO, Proposed_TR_FR_SR and Proposed_TR_FR_SO are very close, respectively. This shows when sampling ratio is extremely low, then there is too little spectrum information available for each algorithm to form a performance gap. Moreover, Proposed_TR_FR_SO is the best compared with Proposed_TR_FS_SO and Proposed_TR_FR_SR. It confirms the efficiency of Proposed_TR_FR_SO in optimizing the spatial sampling position and the assumption that random frequency sampling is better as correlations are weak among different frequency points.

In Fig. 4, we let $r = r_F \cdot r_S$, $r_F = r_S$ and $r_T = 1$, which means there is no compression in time domain. Here the five algorithms are abbreviated as CSOMP_T1, GOMP_T1, Proposed_T1R_FR_SR, Proposed_T1R_FS_SO and Proposed_T1R_FR_SO, respectively. It is evident that the time domain sampling is much more important than the frequency domain and the space domain samplings for the same total sampling rate r , as more sampling points in the time domain greatly decrease the situation recovery error for all algorithms.

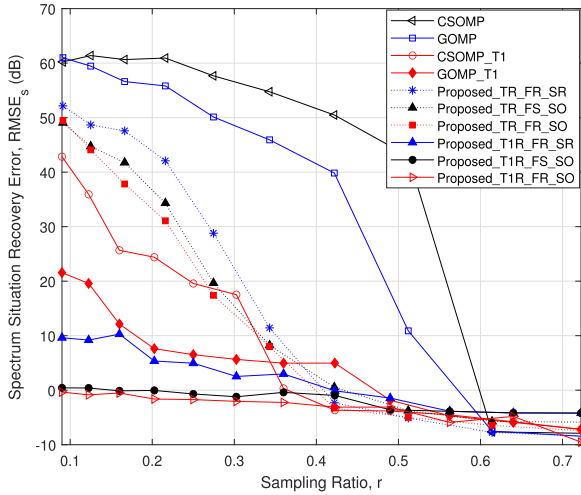


Fig. 4. 3D wideband spectrum situation recovery performance comparisons of the proposed and the comparison algorithms ($r_F = r_S, r_T = 1$).

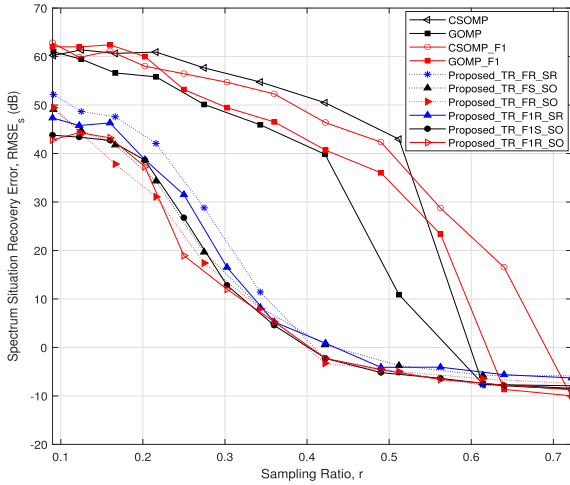


Fig. 5. 3D wideband spectrum situation recovery performance comparisons of the proposed and the comparison algorithms ($r_T = r_S, r_F = 1$).

Besides, when $r_T = 1$, the compressed sampling of space and frequency no longer involves the domain transformation, but becomes the missing values completion in the same domain, which also brings a great improvement to the performance. What's more, similar to the Fig. 3, the Proposed_T1R_FR_SO still outperforms other algorithms in spectrum situation recovery.

In Fig. 5, it sets $r = r_T \cdot r_S$, $r_T = r_S$ and $r_F = 1$ for the spectrum situation recovery performance comparisons. It shows that more frequency sampling points improve the accuracy of situation recovery for CSOMP and Proposed_TR_FR_SR at small r but reduce the performance with large r . With $r_F = 1$, for the Proposed_TR_FS_SO and Proposed_TR_FR_SO, they don't change much, while the performance of GOMP even gets worse. These results suggest that increasing the proportion of frequency sampling in the total sampling rate has little performance improvement.

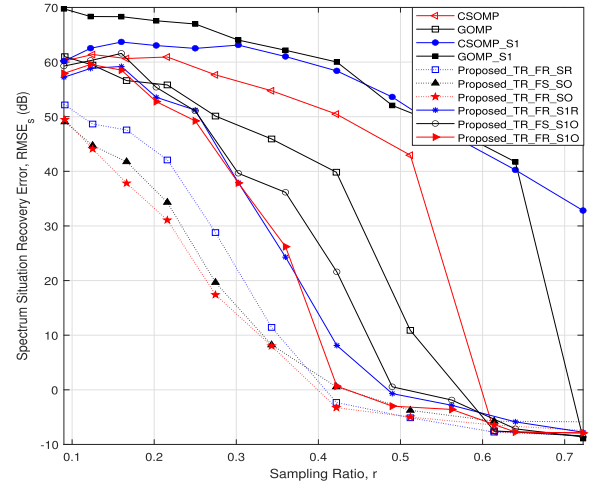


Fig. 6. 3D wideband spectrum situation recovery performance comparisons of the proposed and the comparison algorithms ($r_T = r_F, r_S = 1$).

Moreover, Fig. 6 presents the situation recovery performance of $r = r_T \cdot r_F$, $r_T = r_F$ and $r_S = 1$, which means all the spatial points are sampled. According to the results, it shows that a larger proportion of spatial sampling will lead to a decrease in the performance of spectrum situation recovery, which in turn shows that the samplings in the time and frequency domains are more important.

Totally speaking, the Proposed_TR_FR_SO under different parameter settings is always the best. Large proportion of time domain sampling in the total samplings also contributes to the overall performance improvement. Considering the trade-off between computational complexity and 3D wideband spectrum mapping performance, if excellent performance and recovery stability need to be guaranteed, Proposed_TR_FR_SO scheme is preferred. When the performance and stability requirements are low, along with more demands of spectrum data processing efficiency, it is recommended to adopt Proposed_TR_FR_SR as it doesn't need to optimize the spatial sampling points.

C. Comparison of Signal Strength Recovery Performance

In this subsection, the source signal strength recovery performances are compared among Proposed_TR_FR_SR, Proposed_TR_FS_SO, Proposed_TR_FR_SO, CSOMP and GOMP under different parameter settings. The signal strength recovery mean square error MSE_{ss} is

$$MSE_{ss} = \frac{1}{nq} \sum_{i=1}^{nq} \left| \widehat{\mathbf{s}}_f^{(i)} - \mathbf{s}_f^{(i)} \right|^2, \quad (40)$$

where $\widehat{\mathbf{s}}_f^{(i)}$ and $\mathbf{s}_f^{(i)}$ denote the estimated and true sources signal strengths, respectively. Results are shown in Fig. 7: Increasing the frequency sampling ratio will bring the best signal recovery performance, while large time sampling ratio will result in the worst. Generally speaking, the signal recovery performance is opposite to that of spectrum situation. This is mainly caused by the severe environment shadowing and blocking. Because if small spectrum situation recovery error is desired, the

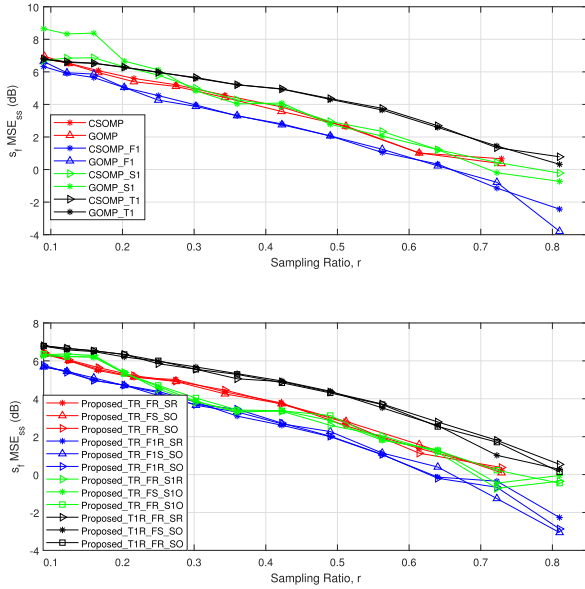


Fig. 7. 3D wideband spectrum source signal strength recovery performance comparisons of the proposed and the comparison algorithms.

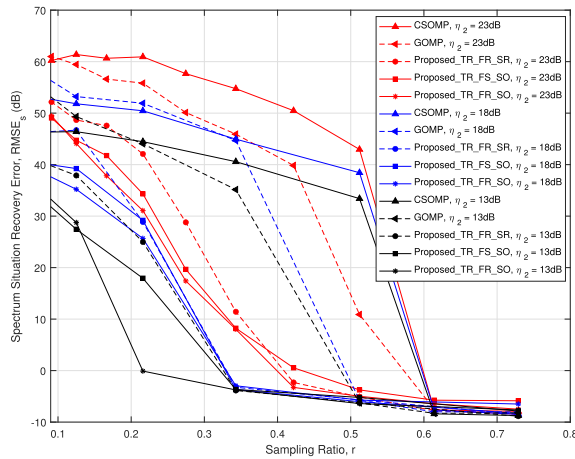


Fig. 8. Impact of η_2 on the spectrum situation recovery performances of the proposed and comparison algorithms.

signal estimation result will inevitably contain the extra fading and noise. Thereby, when both the signal and spectrum situation recovery accuracies need to be guaranteed, the proportion of frequency sampling can be increased according to Fig. 5.

D. Impact of the Excessive Path Loss Coefficient η_2

Here we study the influence of environment parameter η_2 on the performance of spectrum situation recovery for all algorithms as Fig. 8. The value of η_2 are 23 dB, 18 dB and 13 dB. The sampling ratio $r = r_T \cdot r_F \cdot r_S$, $r_T = r_F = r_S$. It can be found that with the reduction of environment parameter η_2 , the spectrum situation recovery performance of each algorithm gets improved. Besides, the Proposed_TR_FR_SO always keeps the optimal which reflects its stability in different spectrum environments.

V. CONCLUSION

This paper addressed the issue of 3D wideband spectrum mapping in a spectrum heterogeneous environment, which contributed to more efficient spectrum management. By taking advantage of the underlying sparsity, 3D wideband spectrum mapping was first formulated as a compressed sensing optimization problem. We executed sampling compressions in three domains of time, frequency and space. In the space domain, QR block pivoting optimization was implemented to obtain dominant sampling locations and showed better performance than random measurements. In the frequency domain, random sampling was preferred as the coherences among frequency points were usually weak. In the time domain, sub-Nyquist sampling further reduced the sampling cost. In the 3D wideband spectrum situation recovery phase, ADMM was applied to obtain the sparse solution. Additionally, we evaluated the recovery performance among the traditional and proposed schemes. Results showed the superiority of the proposed 3D compressed wideband spectrum mapping scheme against traditional algorithms. In the future, more research will be conducted including data-driven basis representation learning and constraints related spectrum mapping, e.g., sampling time limitation and energy consumption of spectrum-monitoring devices.

REFERENCES

- [1] Z. Feng, C. Qiu, Z. Feng, Z. Wei, W. Li, and P. Zhang, "An effective approach to 5G: Wireless network virtualization," *IEEE Commun. Lett.*, vol. 53, no. 12, pp. 53–59, Dec. 2015.
- [2] Q. Wu, G. Ding, J. Wang, and Y. Yao, "Spatial-temporal opportunity detection for spectrum-heterogeneous cognitive radio networks: Two-dimensional sensing," *IEEE Trans. Wirel. Commun.*, vol. 12, no. 2, pp. 516–526, Feb. 2013.
- [3] S. Stotas and A. Nallanathan, "On the throughput and spectrum sensing enhancement of opportunistic spectrum access cognitive radio networks," *IEEE Trans. Wirel. Commun.*, vol. 11, no. 1, pp. 97–107, Jan. 2012.
- [4] P. J. Kolodzy, "Spectrum policy task force report," FCC, Washington, DC, USA, Tech. Rep. 02-135, Nov. 2002.
- [5] M. K. Powell, "Facilitating opportunities for flexible, efficient, and reliable spectrum use employing cognitive radio technologies," FCC, Washington, DC, USA, Tech. Rep. 03-108, Dec. 2003.
- [6] S. Haykin, "Cognitive radio: Brain-empowered wireless communications," *IEEE J. Sel. Areas Commun.*, vol. 23, no. 2, pp. 201–220, Feb. 2005.
- [7] J. Mitola and G. Q. Maguire, "Cognitive radio: Making software radios more personal," *IEEE Pers. Commun.*, vol. 6, no. 4, pp. 13–18, Aug. 1999.
- [8] B. Wang and K. R. Liu, "Advances in cognitive radio networks: A survey," *IEEE J. Sel. Top. Signal Process.*, vol. 5, no. 1, pp. 5–23, Feb. 2011.
- [9] Y. Chen, G. Yu, Z. Zhang, H.-h. Chen, and P. Qiu, "On cognitive radio networks with opportunistic power control strategies in fading channels," *IEEE Trans. Wireless Commun.*, vol. 7, no. 7, pp. 2752–2761, Jul. 2008.
- [10] J. Wang, G. Ding, Q. Wu, L. Shen, and F. Song, "Spatial-temporal spectrum hole discovery: A hybrid spectrum sensing and geolocation database framework," *Chin. Sci. Bull.*, vol. 59, no. 16, pp. 1896–1902, 2014.
- [11] Y. C. Liang, Q. Zhang, E. G. Larsson, and G. Y. Li, "Symbiotic radio: Cognitive backscattering communications for future wireless networks," *IEEE Trans. Cognit. Commun. Netw.*, vol. 6, no. 4, pp. 1242–1255, Dec. 2020.
- [12] J. Schuette et al., "Performance of RF mapping using opportunistic distributed devices," in *Proc. IEEE Conf. Mil. Commun.*, Tampa, FL, USA, 2015, pp. 1624–1629.
- [13] A. B. H. Alaya-Feki, S. B. Jemaa, B. Sayrac, P. Houze, and E. Moulines, "Informed spectrum usage in cognitive radio networks: Interference cartography," in *Proc. IEEE 19th Int. Symp. Pers. Indoor Mobile Radio Commun.*, Cannes, France, 2008, pp. 1–5.

- [14] G. Ding, J. Wang, Q. Wu, Y.-D. Yao, F. Song, and T. A. Tsiftsis, "Cellular-base-station-assisted device-to-device communications in TV white space," *IEEE J. Sel. Areas Commun.*, vol. 34, no. 1, pp. 107–121, Jan. 2016.
- [15] Z. Quan, S. Cui, A. H. Sayed, and H. V. Poor, "Optimal multiband joint detection for spectrum sensing in cognitive radio networks," *IEEE Trans. Signal Process.*, vol. 57, no. 3, pp. 1128–1140, Mar. 2009.
- [16] Z. Tian and G. B. Giannakis, "A wavelet approach to wideband spectrum sensing for cognitive radios," in *Proc. 1st Int. Conf. Cognit. Radio-Oriented Wirel. Netw. Commun.*, Mykonos, Greece, 2006, pp. 1–5.
- [17] H. Landau, "Necessary density conditions for sampling and interpolation of certain entire functions," *Acta Mathematica*, vol. 117, no. 1, pp. 37–52, 1967.
- [18] E. J. Candès and M. B. Wakin, "An introduction to compressive sampling," *IEEE Signal Process. Mag.*, vol. 25, no. 2, pp. 21–30, 2008.
- [19] D. L. Donoho, "Compressed sensing," *IEEE Trans. Inf. Theory*, vol. 52, no. 4, pp. 1289–1306, Apr. 2006.
- [20] E. Candes and T. Tao, "Near-optimal signal recovery from random projections: Universal encoding strategies," *IEEE Trans. Inf. Theory*, vol. 52, no. 12, pp. 5406–5425, Dec. 2006.
- [21] Z. Tian and G. B. Giannakis, "Compressed sensing for wideband cognitive radios," in *Proc. IEEE Int. Conf. Acoust. Speech Signal Process.*, Honolulu, HI, USA, 2007, pp. 1357–1360.
- [22] M. Elad, "Optimized projections for compressed sensing," *IEEE Trans. Signal Process.*, vol. 55, no. 12, pp. 5695–5702, Dec. 2007.
- [23] V. Atanasovski et al., "Constructing radio environment maps with heterogeneous spectrum sensors," in *Proc. IEEE Int. Symp. Dyn. Spectr. Access Netw.*, Aachen, Germany, 2011, pp. 660–661.
- [24] G. Ding, Q. Wu, Y. Yao, J. Wang, and Y. Chen, "Kernel-based learning for statistical signal processing in cognitive radio networks: Theoretical foundations, example applications, and future directions," *IEEE Signal Process. Mag.*, vol. 30, no. 4, pp. 126–136, Jul. 2013.
- [25] D. Romero, S. Kim, G. B. Giannakis, and R. Lopez-Valcarce, "Learning power spectrum maps from quantized power measurements," *IEEE Trans. Signal Process.*, vol. 65, no. 10, pp. 2547–2560, May 2017.
- [26] X. Han, L. Xue, F. Shao, and Y. Xu, "A power spectrum maps estimation algorithm based on generative adversarial networks for underlay cognitive radio networks," *Sensors*, vol. 20, Jan. 2020, Art. no. 311.
- [27] J. Sun et al., "Long-term spectrum state prediction: An image inference perspective," *IEEE Access*, vol. 6, pp. 43489–43498, 2018.
- [28] C. Ge, Z. Wang, and X. Zhang, "Robust long-term spectrum prediction with missing values and sparse anomalies," *IEEE Access*, vol. 7, pp. 16655–16664, 2019.
- [29] F. Shen, G. Ding, Z. Wang, and Q. Wu, "UAV-based 3D spectrum sensing in spectrum-heterogeneous networks," *IEEE Trans. Veh. Technol.*, vol. 68, no. 6, pp. 5711–5722, Jun. 2019.
- [30] Q. Wu, F. Shen, Z. Wang, and G. Ding, "3D spectrum mapping based on ROI-driven UAV deployment," *IEEE Netw.*, vol. 34, no. 5, pp. 24–31, Sep./Oct. 2020.
- [31] K. Manohar, B. W. Brunton, J. N. Kutz, and S. L. Brunton, "Data-driven sparse sensor placement for reconstruction: Demonstrating the benefits of exploiting known patterns," *IEEE Control Syst. Mag.*, vol. 38, no. 3, pp. 63–86, Jun. 2018.
- [32] E. Candes, J. Romberg, and T. Tao, "Robust uncertainty principles: Exact signal reconstruction from highly incomplete frequency information," *IEEE Trans. Inf. Theory*, vol. 52, no. 2, pp. 489–509, Feb. 2006.
- [33] E. Candes and T. Tao, "Decoding by linear programming," *IEEE Trans. Inf. Theory*, vol. 51, no. 12, pp. 4203–4215, Dec. 2005.
- [34] E. Candes, "The restricted isometry property and its implications for compressed sensing," *Comptes Rendus Mathematique*, vol. 346, no. 9–10, pp. 589–592, May 2008.
- [35] E. Candes and J. Romberg, "Sparsity and incoherence in compressive sampling," *Inverse Problems*, vol. 23, no. 3, pp. 969–985, Apr. 2007.
- [36] Y. Wang, Z. Tian, and C. Feng, "Collecting detection diversity and complexity gains in cooperative spectrum sensing," *IEEE Trans. Wirel. Commun.*, vol. 11, no. 8, pp. 2876–2883, Aug. 2012.
- [37] F. Shen, Z. Wang, G. Ding, K. Li, and Q. Wu, "3D compressed spectrum mapping with sampling locations optimization in spectrum-heterogeneous environment," *IEEE Trans. Wirel. Commun.*, vol. 21, no. 1, pp. 326–338, Jan. 2022.
- [38] H. Sun, W. Chiu, and A. Nallanathan, "Adaptive compressive spectrum sensing for wideband cognitive radios," *IEEE Commun. Lett.*, vol. 16, no. 11, pp. 1812–1815, Nov. 2012.
- [39] Z. Qin, Y. Gao, M. D. Plumbley, and C. G. Parini, "Wideband spectrum sensing on real-time signals at sub-nyquist sampling rates in single and cooperative multiple nodes," *IEEE Trans. Signal Process.*, vol. 64, no. 12, pp. 3106–3117, Jun. 2016.
- [40] Z. Qin, X. Zhou, L. Zhang, Y. Gao, Y.-C. Liang, and G. Y. Li, "20 years of evolution from cognitive to intelligent communications," *IEEE Trans. Cognit. Commun. Netw.*, vol. 6, no. 1, pp. 6–20, Mar. 2019.
- [41] Z. Wang and C. Ling, "On the geometric ergodicity of Metropolis-Hastings algorithms for lattice Gaussian sampling," *IEEE Trans. Inf. Theory*, vol. 64, no. 2, pp. 738–751, Feb. 2018.
- [42] Z. Wang and C. Ling, "Lattice Gaussian sampling by Markov chain monte carlo: Bounded distance decoding and trapdoor sampling," *IEEE Trans. Inf. Theory*, vol. 65, no. 6, pp. 3630–3645, Jun. 2019.
- [43] M. Mozaffari, W. Saad, M. Bennis, and M. Debbah, "Mobile unmanned aerial vehicles (UAVs) for energy-efficient Internet of Things communications," *IEEE Trans. Wirel. Commun.*, vol. 16, no. 11, pp. 7574–7589, Nov. 2017.
- [44] T. F. Chan, "Rank revealing QR factorizations," *Linear Algebra Appl.*, vol. 88–89, Apr. 1987, pp. 67–82.
- [45] J. A. Duersch and M. Gu, "Randomized QR with column pivoting," *SIAM J. Sci. Comput.*, vol. 39, no. 4, pp. C263–C291, Jan. 2017.
- [46] T. F. Chan and P. C. Hansen, "Some applications of the rank revealing QR factorization," *SIAM J. Sci. Statist. Comput.*, vol. 13, no. 3, pp. 727–741, May 1992.
- [47] P. Businger and G. H. Golub, "Linear least squares solutions by householder transformations," *Numerische Mathematik*, vol. 7, no. 3, pp. 269–276, Jun. 1965.
- [48] A. Sommariva and M. Vianello, "Computing approximate fekte points by QR factorizations of vandermonde matrices," *Comput. Math. Appl.*, vol. 57, no. 8, pp. 1324–1336, Apr. 2009.
- [49] Z. Drmac and S. Gugercin, "A new selection operator for the discrete empirical interpolation method-improved a priori error bound and extensions," *SIAM J. Sci. Comput.*, vol. 38, no. 2, pp. A631–A648, May 2016.
- [50] S. Boyd, N. Parikh, E. Chu, B. Peleato, and J. Eckstein, *Distributed Optimization and Statistical Learning Via the Alternating Direction Method of Multipliers*. Delft, The Netherlands: Now Publishers, 2011, pp. 1–122.
- [51] J. A. Tropp and A. C. Gilbert, "Signal recovery from random measurements via orthogonal matching pursuit," *IEEE Trans. Inf. Theory*, vol. 53, no. 12, pp. 4655–4666, Dec. 2007.
- [52] J. Wang, S. Kwon, and B. Shim, "Generalized orthogonal matching pursuit," *IEEE Trans. Signal Process.*, vol. 60, no. 12, pp. 6202–6216, Dec. 2012.



Feng Shen received the B.S. degree in information engineering from the Nanjing University of Aeronautics and Astronautics, Nanjing, China, in 2017. He is currently working toward the Ph.D. degree with the College of Electronics and Information Engineering, Nanjing University of Aeronautics and Astronautics, Nanjing, China. His research interests include spectrum mapping, cognitive information theory, cognitive radio, signal processing, and wireless communications.



Guoru Ding (Senior Member, IEEE) received the B.S. (with Hons.) degree in electrical engineering from Xidian University, Xi'an, China, in 2008, and the Ph.D. (with Hons.) degree in communications and information systems from the College of Communications Engineering, Nanjing, China, in 2014. He is currently an Associate Professor with the College of Communications Engineering. His research interests include cognitive radio networks, massive MIMO, machine learning, and Big Data analytics over wireless networks. He is also an Associate Editor for the

IEEE TRANSACTIONS ON COGNITIVE COMMUNICATIONS AND NETWORKING. He was a Guest Editor of the IEEE JOURNAL ON SELECTED AREAS IN COMMUNICATIONS SPECIAL ISSUE ON SPECTRUM SHARING AND AGGREGATION IN FUTURE WIRELESS NETWORKS.



Qihui Wu (Senior Member, IEEE) received the B.S. degree in communications engineering, and the M.S. and Ph.D. degrees in communications and information systems from the Institute of Communications Engineering, Nanjing, China, in 1994, 1997, and 2000, respectively. From 2003 to 2005, he was a Postdoctoral Research Associate with Southeast University, Nanjing, China. From 2005 to 2007, he was an Associate Professor with the College of Communications Engineering, PLA University of Science and Technology, Nanjing, China, where he was a Full

Professor from 2008 to 2016. Since May 2016, he has been a Full Professor with the College of Electronic and Information Engineering, Nanjing University of Aeronautics and Astronautics, Nanjing, China. From March 2011 to September 2011, he was an Advanced Visiting Scholar in Stevens Institute of Technology, Hoboken, USA. His research interests include wireless communications and statistical signal processing, with emphasis on system design of software defined radio, cognitive radio, and smart radio.



Zheng Wang (Member, IEEE) received the B.S. degree in electronic and information engineering from the Nanjing University of Aeronautics and Astronautics, Nanjing, China, in 2009, the M.S. degree in communications from the Department of Electrical and Electronic Engineering, University of Manchester, Manchester, U.K., in 2010 and the Ph.D degree in communication engineering from Imperial College London, London, U.K., in 2015. He is currently an Associate Professor with the School of Information Science and Engineering, Southeast University, Nan-

jing, China. His research interests include lattice methods for wireless communications, machine learning, and intelligent technology for communications.